doi:10.1093/jmcb/mjy067
Published online November 14, 2018

Article

Chlamydomonas WDR92 in association with R2TP-like complex and multiple DNAAFs to regulate ciliary dynein preassembly

Guang Liu[1], Limei Wang[1], and Junmin Pan[1,2,*]

[1] MOE Key Laboratory of Protein Sciences, Tsinghua-Peking Center for Life Sciences, School of Life Sciences, Tsinghua University, Beijing 100084, China
[2] Laboratory for Marine Biology and Biotechnology, Qingdao National Laboratory for Marine Science and Technology, Qingdao 266200, China
* Correspondence to: Junmin Pan, E-mail: panjunmin@tsinghua.edu.cn

Edited by Xuebiao Yao

The motility of cilia or eukaryotic flagella is powered by the axonemal dyneins, which are preassembled in the cytoplasm by proteins termed dynein arm assembly factors (DNAAFs) before being transported to and assembled on the ciliary axoneme. Here, we characterize the function of WDR92 in *Chlamydomonas*. Loss of WDR92, a cytoplasmic protein, in a mutant *wdr92* generated by DNA insertional mutagenesis resulted in aflagellate cells or cells with stumpy or short flagella, disappearance of axonemal dynein arms, and diminishment of dynein arm heavy chains in the cytoplasm, suggesting that WDR92 is a DNAAF. Immunoprecipitation of WDR92 followed by mass spectrometry identified inner dynein arm heavy chains and multiple DNAAFs including RuvBL1, RPAP3, MOT48, ODA7, and DYX1C. The PIH1 domain-containing protein MOT48 formed a R2TP-like complex with RuvBL1/2 and RPAP3, while PF13, another PIH1 domain-containing protein with function in dynein preassembly, did not. Interestingly, the third PIH1 domain-containing protein TWI1 was not related to flagellar motility. WDR92 physically interacted with the R2TP-like complex and the other identified DNNAFs. Our data suggest that WDR92 functions in association with the HSP90 co-chaperone R2TP-like complex as well as linking other DNAAFs in dynein preassembly.

Keywords: cilia motility, dynein arm assembly factors, R2TP complex, WDR92, *Chlamydomonas*

Introduction

The motility of cilia is driven by the outer dynein arms (ODAs) and inner dynein arms (IDAs) that localize with a characteristic spatial periodicity on the axonemal microtubules. ODAs and IDAs are large protein complexes composed of distinct dynein heavy chains and multiple accessory subunits (Kamiya and Yagi, 2014; Ishikawa, 2017). Accumulative evidences suggest that the ODAs and IDAs complexes are initially preassembled in the cytoplasm followed by transport via intraflagellar transport (IFT) and anchoring to the ciliary axoneme (Fok et al., 1994; Fowkes and Mitchell, 1998; Ahmed et al., 2008; Zhang, et al., 2019).

At least a dozen proteins are known or suspected to be factors involved in the preassembly process and termed dynein arm assembly factors (DNAAFs) (Mitchison et al., 2012; Desai et al., 2018). These assembly factors are cytoplasmic, and when their function is compromised, related dynein arm heavy chains are diminished in the cytoplasm and ODAs and/or IDAs are lost from the ciliary axoneme. Axonemal dynein heavy chains are massive proteins consisting of >4000 residues and the axonemal dynein may comprise >20 components (Kato et al., 2014; King, 2016). The folding of large proteins as well as assembly of large protein complexes requires molecular chaperones (Kakihara and Houry, 2012; Balchin et al., 2016). Thus, the divergent assembly factors may form a complex to bring various dynein components as clients to the chaperones for folding as well as for assembly of the dynein complex.

R2TP complex is a HSP90 co-chaperone and comprises Rvb1, Rvb2, Tah1, and Pih1 in yeast, or RuvBL1, RuvBL2, RPAP3, and PIH1D1 in mammals (Kakihara and Houry, 2012). It was initially identified in genome-wide screens in yeast for HSP90 interacting proteins and subsequently discovered in mammals (Zhao et al., 2005;

Received September 20, 2018. Revised October 30, 2018. Accepted November 13, 2018.

Te et al., 2007). R2TP is involved in the assembly of large protein complexes such as RNA polymerase II, small nucleolar ribonucleoproteins (snoRNPs), and protein complexes associated with phosphatidylinositol 3 kinase-related kinases (PIKKs) (Kakihara and Houry, 2012). Recent advances suggest that it also functions in dynein preassembly as revealed by analysis of alteration of genes encoding R2TP components and/or their homologs in various ciliated organisms (Omran et al., 2008; Yamamoto et al., 2010; Knowles et al., 2013; Zhao et al., 2013; Dong et al., 2014; Li et al., 2017; Olcese et al., 2017; Paff et al., 2017; Yamaguchi et al., 2018; Zur Lage et al., 2018).

WDR92, previously known as Monad, is a WD40-repeat protein with seven repeats forming a 7-bladed toroidal β-propeller structure and was initially shown to be involved in apoptosis (Saeki et al., 2006; Patel-King and King, 2016). Subsequent experiments show that WDR92 interacts with the components of the R2TP complex, suggesting its possible role in protein folding and maturation of protein complexes (Itsuki et al., 2008; Cloutier et al., 2009; Boulon et al., 2010; Houry et al., 2018). Impairments of *WDR92* gene expression in planaria and fly both result in loss of dynein arms among other ciliary defects (Patel-King and King, 2016; Zur Lage et al., 2018). However, the mechanism by which WDR92 regulates dynein arm preassembly remains to be fully elucidated.

In this study, we have characterized a *Chlamydomonas wdr92* mutant, which is aflagellate or has short or stumpy flagella lacking both dynein arms. The ODA heavy chains DHCα and DHCβ, and IDA heavy chains DHC5, DHC8, and DHC9 are diminished in the cytoplasm. WDR92, a cytoplasmic protein, is associated with a R2TP-like complex formed by RuvBL1, RuvBL2, MOT48, and RPAP3 as well as with dynein assembly factors ODA7, FBB18, and DYX1C. Thus, WDR92 links R2TP complex and other assembly factors to function in dynein arm preassembly.

Results

Generation and characterization of a wdr92 mutant in Chlamydomonas

We have used DNA insertional mutagenesis to screen for mutants defective in flagellar formation. In contrast to wild-type (WT) cells that have flagella of around 12 μm long, one of the identified mutants was either aflagellate or had short or stumpy flagella (Figure 1A). Furthermore, the mutant cells with short flagella were immotile. By using restriction enzyme site-directed PCR (RESDA-PCR) followed by sequencing and BLAST (Gonzalez-Ballester et al., 2005), the foreign DNA fragment was found to be inserted into the third exon of *WDR92* with depletion of two nucleotides (556 and 557 nt) (Figure 1B). WDR92 is highly conserved in organism with motile cilia (Patel-King and King, 2016).

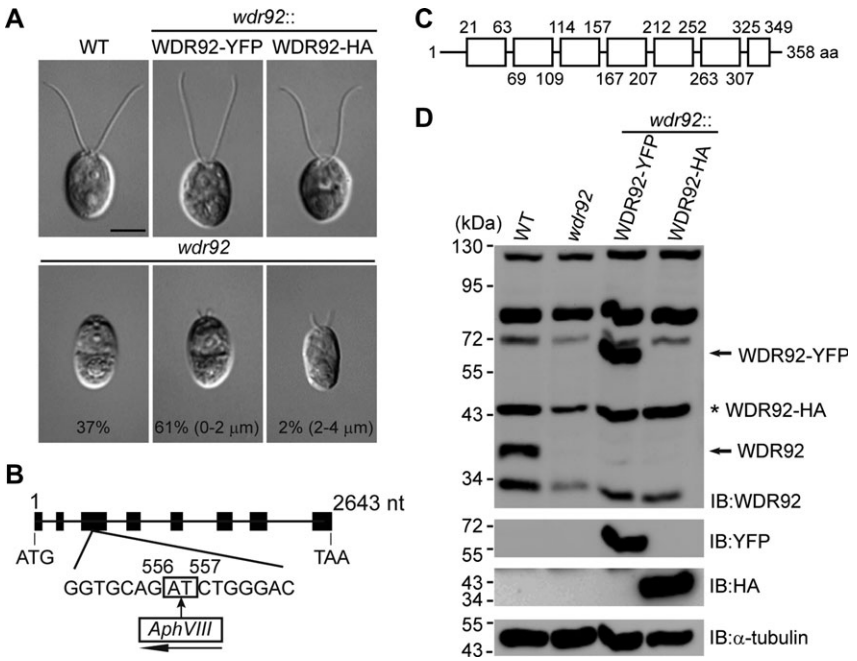

Figure 1 Isolation and characterization of a *wdr92* mutant. (**A**) *wdr92* is defective in flagellar assembly and can be rescued by expression of the endogenous gene. DIC images show the flagellar phenotypes of WT, mutant, and the rescued cells. *WDR92* tagged with YFP or HA at the C-terminus was transformed into *wdr92* to rescue the mutant. Scale bar, 5 μm. (**B**) Schematic presentation of the *WDR92* gene structure with foreign DNA insertion site. The insertion of a foreign DNA fragment (*AphVIII*) in the third exon of the gene replaces two nucleotides (556–557 nt). The arrow underneath the boxed *AphVIII* shows the direction of the insertion from 5′ to 3′ end. (**C**) Diagram showing the protein structure of WDR92. Boxed regions indicate the WD repeat domains as predicted from NCBI protein BLAST. Please note that the last WD repeat is partial. (**D**) Immunoblot analysis of *WDR92* expression in the WT, mutant, and the rescued cells. Cell lysates from the cell samples as indicated were subjected to immunoblotting using the indicated antibodies. *The unspecific band is overlapped with WDR92-HA.

Chlamydomonas WDR92 (Cre16.g672600) encodes a protein of 358 aa with molecular weight of 39664 and a PI of 6.51. It has six intact WD repeats and one partial repeat (Figure 1C).

To examine whether DNA insertion disrupted the expression of *WDR92* in this mutant, a polyclonal antibody was generated to assess its expression by immunoblotting in WT and mutant cells. A protein band similar to the predicted molecular weight of WDR92 was detected in WT cells but not in the mutant (Figure 1D), suggesting that DNA insertional mutation disrupts the expression of WDR92. To determine whether the mutant phenotypes were consequences of *WDR92* mutation, *wdr92* mutant cells were transformed with *WDR92* tagged with YFP or HA at the C-terminus. Transformants that expressed recombinant proteins all rescued the flagellar phenotypes of *wdr92* (Figure 1A and D), indicating that *WDR92* is the causal gene.

WDR92 is cytoplasmic and its mutation results in loss of axonemal dynein arms and cytoplasmic dynein heavy chains

In fly and planaria, WDR92 was implicated in dynein arm preassembly (Patel-King and King, 2016; Zur Lage et al., 2018). Next, we examined whether *WDR92* mutation affected dynein arm assembly in the flagella by electron thin-section microscopy. In contrast to the WT flagella, the dynein arms including ODA and IDA were not detected in the mutant (Figure 2A). Loss of dynein arms may be due to defects in anchoring and assembly of dynein arms in the axoneme (Hjeij et al., 2014; Wallmeier et al., 2016), its transport from cell body to the flagella (Ahmed et al., 2008) or dynein preassembly (Desai et al., 2018). We first examined the cellular location of WDR92. Cells expressing WDR92-HA were examined by immunostaining analysis using the HA antibody. WDR92 displayed a punctate localization pattern in the cytoplasm and no staining was observed in the flagella (Figure 2B). Immunoblotting of isolated cell body and flagella showed that WDR92 was exclusively localized in the cell body (Figure 2C), suggesting that WDR92 functions in the cell body. *Chlamydomonas* has three ODA heavy chains (DHCα, DHCβ, and DHCγ) and 12 IDA heavy chains (Yagi et al., 2009; Kamiya and Yagi, 2014). To determine whether WDR92 affected dynein preassembly, cell lysates from WT, mutant and the rescued cells were subjected to immunoblot analysis for representative dynein components (Figure 2D). The outer arm dynein intermediate chain IC2 in the mutant was slightly reduced relative to the WT cell. Remarkably, ODA heavy chains DHCα and DHCβ, and IDA heavy chains DHC5, DHC8, and DHC9 were not detectable in the mutant. To determine the loss of dynein heavy chains was not due to defect in their gene expression, RT-PCR was performed. As shown in Figure 2E, the mRNAs of these heavy chains were detected. These results indicate that WDR92 is involved in ODA and IDA preassembly.

WDR92 associates with IDA heavy chains and several DNAAFs

To learn about the potential working mechanism of WDR92, cells expressing WDR92-YFP were subjected to immunoprecipitation with the GFP antibody. The immunoprecipitates were analyzed on SDS-PAGE and the gel slices were analyzed by mass spectrometry (Supplementary Figure S1). We found that several IDA heavy

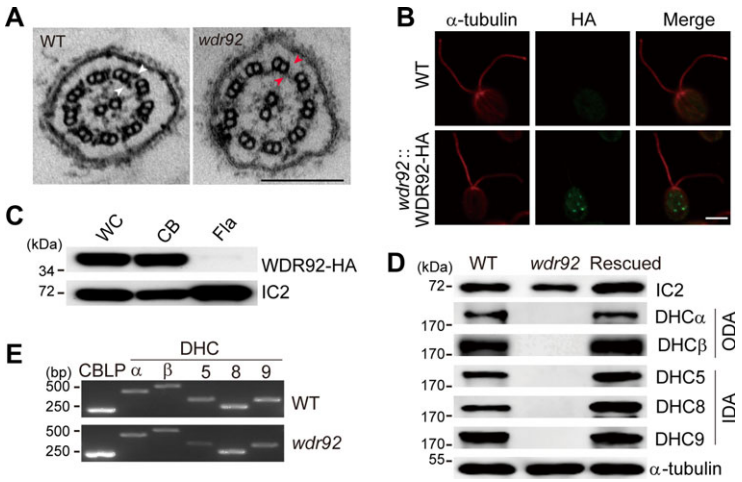

Figure 2 WDR92 is cytoplasmic and its loss results in disappearance of axonemal dynein arms and diminishment of dynein arm heavy chains in the cytoplasm. (**A**) Loss of ODAs and IDAs in *wdr92* flagella. Representative EM cross-sections of WT and *wdr92* flagella are shown. White arrow heads indicate ODA (upper, right) and IDA (lower, right), respectively. Red arrow heads indicate the positions of ODA (upper, right) and IDA (lower, right) in the mutant. Scale bar, 200 nm. (**B**) WDR92 is cytoplasmic. WT and rescued cells expressing *WDR92-HA* were immunostained with HA and α-tubulin antibodies. Scale bar, 5 μm. (**C**) Immunoblot analysis of WDR92 in the cell body and flagella. Equal amounts of proteins from whole cell (WC), cell body (CB), and flagella (Fla) were analyzed with the indicated antibodies. IC2, an intermediate chain of outer arm dynein was used as a control. (**D**) Dynein heavy chains from ODAs and IDAs are undetectable in the cytoplasm of *wdr92*. Cell lysates from WT, *wrd92*, and the rescued cells were analyzed by immunoblotting using the indicated antibodies against representative dynein heavy chains from ODAs or IDAs. (**E**) Expression of dynein heavy chains in WT and *wdr92* cells. RT-PCR was performed to examine the expression of dynein heavy chains as indicated. The expression of *CBLP* was used as a control.

chains were at least twice enriched in the WDR92-YFP immunoprecipitates relative to the control (Table 1). Interestingly, no enriched ODA components were found. In addition, we found several known factors involved in dynein preassembly. DNAAF1/ODA7 is involved in ODA preassembly (Duquesnoy et al., 2009; Mitchison et al., 2012). Interestingly, in addition to ODA7, we also found a homolog of ODA7 (Table 1). Thus, we termed ODA7 as ODA7a and the newly found homolog as ODA7b. However, the function of ODA7b is not known. Mutations in *DNAAF4/DYX1C/PF23* result in loss of the majority of IDAs and a fraction of ODA in *Chlamydomonas* flagella (Yamamoto et al., 2017). MOT48 functions in preassembly of IDAs and homologous to the protein interaction with Hsp90 1 (PIH1) domain-containing protein of the R2TP complex (Yamamoto et al., 2010; Yamaguchi et al., 2018). *Chlamdyomonas* RuvBL1 and RPAP3 are homologs of RuvBL1 and RPAP3 of the human R2TP complex, respectively (Maurizy et al., 2018). Though the functions of RuvBL1 and RPAP3 in *Chlamydomonas* are not clear, their homologs are involved in dynein preassembly in zebrafish and fly (Li et al., 2017; Zur Lage et al., 2018). These data indicate that WDR92 associates with these DNAAFs to function in dynein arm preassembly.

Physical interactions of WDR92 with the identified DNAAFs

To learn how WDR92 associates with the identified DNAAFs, we first performed yeast two-hybrid assays. Pair-wise combinations of the proteins as indicated were tested. The results of the control experiments for self-activation are shown in Supplementary Figure S2. WDR92 interacted with RPAP3, which further interacted with MOT48 (Figure 3A). These data are consistent with previous studies. Mammalian WDR92 interacts with RPAP3 and RPAP3 interacts with PIH1 domain-containing proteins while MOT48 is a PIH1-containing protein (Itsuki et al., 2008; Yamamoto et al., 2010; Henri et al., 2018; Martino et al., 2018; Maurizy et al., 2018). MOT48 interacted with DYX1C/PF23 (Figure 3B). In mammalian cells, both PIH1 domain-containing proteins DNAAF2/PF13/Ktu and PIH1D3 interact with DYX1C (Maurizy et al., 2018).

The left-over ODA7a, ODA7b, and RuvBL1 were not found to have interactions with the above factors. ODA7 has been shown to interact with FBB18/C21orf59, a factor involved in dynein arm formation (Jaffe et al., 2016). We reckoned that WDR92 might associate with ODA7 through FBB18. As shown in Figure 3C, WDR92 indeed interacted with FBB18, which further interacted with ODA7a but not ODA7b. Both ODA7a and ODA7b possess a leucine rich repeat domain, suggesting they might be able to interact with each other. As expected, they did interact with each other (Figure 3D). Based on the above data, we have presented an interaction map of these studied proteins (Figure 3E).

To verify the interactions derived from the yeast two-hybrid assays, we have employed GST pull-down assays. Bacterial expressed recombinant proteins as indicated were mixed together followed by GST pull-down analysis. GST was used as a negative control. WDR92 interacted with RPAP3 (Figure 4A), which interacted with MOT48 that further interacted with DYX1C (Figure 4B and C). WDR92 interacted with FBB18, which interacted with ODA7a that further interacted with ODA7b (Figure 4D and E). Thus, two different assays confirm the interaction map shown in Figure 3E.

MOT48 participates in formation of a R2TP-like complex that interacts with WDR92 in vivo

The conventional R2TP complex consists of four components RuvBL1/Rvb1p, RuvBL2/Rvb2p, RPAP3/Tah1p, and the PIH1 domain-containing protein PIH1D1/Pih1p (Kakihara and Houry, 2012). MOT48 is a PIH1 domain-containing protein, and the identification of RPAP3 and RuvBL1 in the WDR92 immunoprecipitate suggests that a R2TP-like complex is likely formed *in vivo*. RuvBL1 and RuvBL2 in mammalian or yeast cells form a heterohexamer that interacts with PIH1D1 and RPAP3 (Rivera-Calzada

Table 1 WDR92-associated proteins.

Group	Protein name	Gene ID	Control spectral count (unique peptides)	WDR92-YFP spectral count (unique peptides)
IDA components	DHC2 (Dynein d)	Cre09.g392282	5 (3)	75 (57)
	DHC4	Cre02.g107350	3 (1)	6 (2)
	DHC5 (Dynein b)	Cre02.g107050	–	42 (27)
	DHC6 (Dynein a)	Cre05.g244250	–	58 (45)
	DHC8 (Dynein e)	Cre16.g685450	–	13 (10)
	DHC9 (Dynein c)	Cre02.g141606	3 (1)	9 (6)
	DHC10	Cre14.g624950	21 (19)	42 (35)
	DHC11	Cre12.g555950	3 (1)	13 (9)
Known factors involved in dynein assembly	DNAAF1/ODA7a	Cre01.g029150	–	7 (5)
	DNAAF1/ODA7b	Cre09.g389300	–	9 (4)
	DNAAF4/DYX1C/PF23	Cre11.g467560	–	11 (10)
	MOT48	Cre10.g467050	–	39 (11)
	RPAP3	Cre02.g084900	–	139 (32)
	RUVBL1	Cre09.g414050	3 (3)	11 (8)
Chaperones	HSP70 (ER type)	Cre02.g080700	7 (1)	15 (6)
	CCT2	Cre09.g416750	10 (8)	63 (28)
	CCT8	Cre03.g168450	8 (6)	41 (22)

Immunoprecipiates from cells expressing WDR92-YFP or control cells were analyzed by mass spectrometry. Dynein components, chaperones, and known factors involved in dynein assembly as reported previously that were enriched at least 2-fold in the sample vs. control are shown.

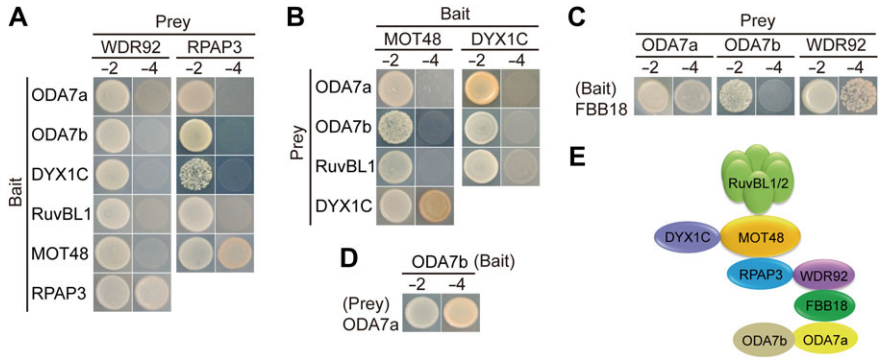

Figure 3 WDR92 associates with multiple DNAAFs. (**A**–**D**) Yeast two-hybrid assays showing the interactions among multiple DNAAFs identified by WDR92 immunoprecipitation combined with mass spectrometric analysis. (**A**) WDR92 interacts with RPAP3, which further interacts with MOT48. (**B**) MOT48 interacts with DYX1C. (**C**) FBB18 interacts with ODA7a and WDR92. (**D**) ODA7a interacts with ODA7b. –2, –Leu/–Trp; –4, –Leu/–Trp/–His/–Ade. (**E**) A diagram showing protein interactions derived from the yeast two-hybrid assays shown above and data shown in Figure 5. Please note, RuvBL1 alone did not interact with any of the proteins immunoprecipitated from WDR92. However, the data shown in Figure 5 demonstrate that RuvBL1/2 heteromer interacts with MOT48.

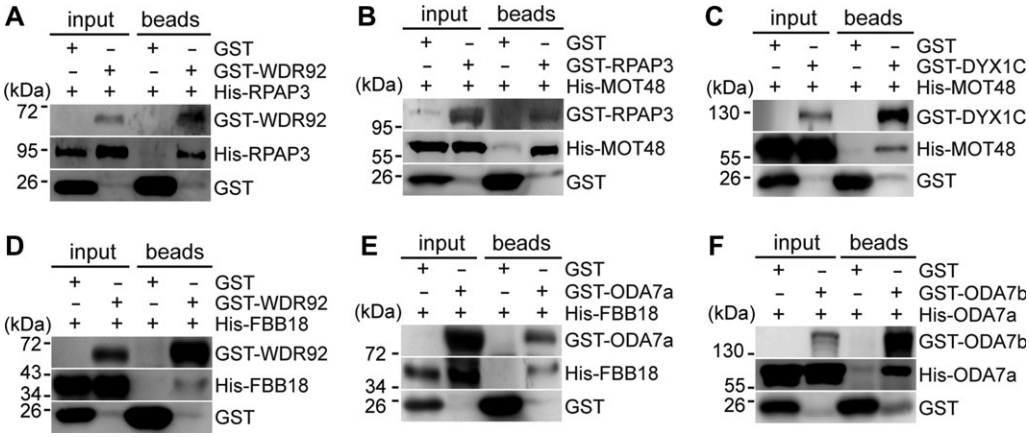

Figure 4 GST pull-down assays confirm the protein interactions demonstrated by yeast two-hybrid assays. (**A**–**F**) Recombinant proteins as indicated were expressed in *Escherichia coli* and mixed together followed by GST pull-down and immunoblot analysis. GST was used as a negative control. Interactions between WDR92 and RPAP3 (**A**), between RPAP3 and MOT48 (**B**), between MOT48 and DYX1C (**C**), between WDR92 and FBB18 (**D**), between FBB18 and ODA7a (**E**), and between ODA7a and ODA7b (**F**).

et al., 2017; Martino et al., 2018; Maurizy et al., 2018). RuvBL1 alone in yeast two-hybrid assay did not show its interaction with MOT48 (Figure 3A). We suspected that only RuvBL1/2 heteromers would interact with MOT48. To demonstrate this, bacterial expressed RuvBL1/2 and MOT48 were mixed in a pull-down assay for protein interactions. Indeed, MOT48 interacted with the heteromers (Figure 5A). In a similar assay, RPAP3 was pulled down with RuvBL1/2 and MOT48, indicating that a R2TP-like complex is formed (Figure 5B). As WDR92 interacted with RPAP3 (Figures 3A and 4A), it likely interacts with the R2TP-like complex. To show this, bacterial expressed WDR92 was mixed with the components of R2TP-like complex followed by GST pull-down assay. Indeed, WDR92 and the components of the R2TP complex were pulled down together, indicating that WDR92 associates with the R2TP-like complex (Figure 5C).

To demonstrate whether WDR92 associated with the R2TP-like complex *in vivo*, cell lysates from WT cells and cells expressing MOT48-HA were subjected to immunoprecipitation with the HA antibody followed by immunoblotting. WDR92 was immunoprecipitated with the components of the R2TP-like complex (Figure 5D). In addition, FBB18 was also detected.

PF13 is unlikely involved in formation of a R2TP-like complex

In *Chlamydomonas*, there are three PIH1 domain-containing proteins that include MOT48, PF13, and TWI1 (Yamamoto et al., 2010). The human homolog Ktu of PF13 forms a R2TP-like complex (RuvBL1/2, SPAG1, and Ktu) (Maurizy et al., 2018). SPAG1 is a paralogue of RPAP3 and functions in dynein assembly while only a single RPAP3 is present in the *Chlamydomonas* proteome (Knowles et al., 2013; Maurizy et al., 2018). As PF13 is also

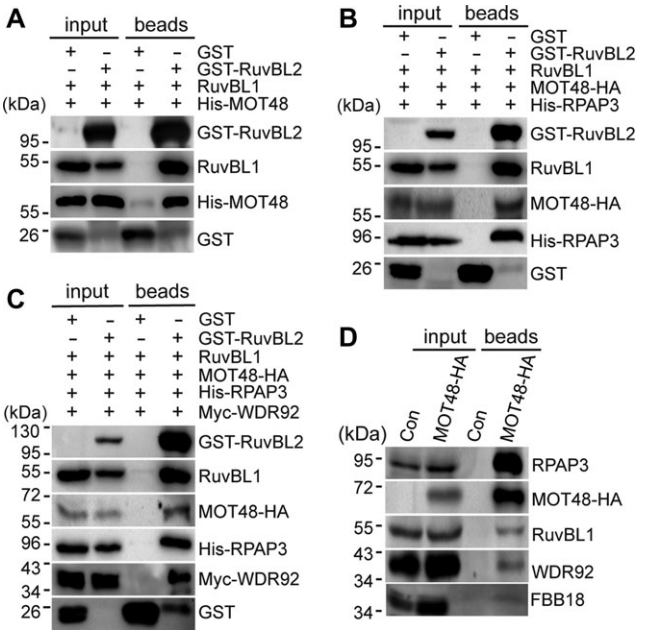

Figure 5 MOT48 is part of a R2TP-like complex that associates with WDR92. (**A**–**C**) GST pull-down assays show that MOT48 is a component of R2TP-like complex that interacts with WDR92. Bacterial expressed proteins were mixed together as indicated followed by GST pull-down and immunoblot analysis. (**A**) MOT48 interacts with RuvBL1/2. (**B**) MOT48 forms a R2TP-like complex with RuvBL1/2 and RPAP3. (**C**) WDR92 associates with the R2TP-like complex. (**D**) WDR92 associates with the R2TP complex shown by immunoprecipitation analysis. WT cells and cells expressing MOT48-HA were immunoprecipitated with anti-HA antibody followed by immunoblot analysis using the indicated antibodies.

involved in dynein arm preassembly (Omran et al., 2008; Mitchison et al., 2012), we wondered whether PF13 might also form a R2TP-like complex. To this end, bacterial expressed proteins PF13, RuvBL1/2, and RPAP3 were mixed together followed by GST pull-down assay. All the proteins were pulled down, indicating that a R2TP-like complex is formed (Figure 6A). We further showed that WDR92 could interact with this complex (Figure 6B). Next, we determined whether this R2TP-like complex actually occurred *in vivo*. Cell lysates from WT cells and cells expressing PF13-HA were subjected to immunoprecipitation with the HA antibody followed by immunoblotting. In contrast to the control, PF13 was immunoprecipitated (Figure 6C). Surprisingly, the rest components of the R2TP-like complex as well as WDR92 were not detected. These data suggest that PF13 is not involved in R2TP-like complex formation *in vivo*. It has been reported that PF13 homolog Ktu forms a complex with DYX1C and HSP90 (Olcese et al., 2017; Maurizy et al., 2018). Consistent with this, we found that PF13 could interact with DYX1C in a pull-down assay though it remains to be determined whether this interaction occurs *in vivo* (Figure 6D).

TWI1 is a homolog of PIH1D3, which is implicated dynein arm preassembly in mouse and zebrafish (Dong et al., 2014; Yamaguchi et al., 2018). Currently, it is not known whether TWI1 has a similar function in *Chlamydomonas*. We examined a *twi1* mutant obtained from the *Chlamydomonas* Resource Center. The *twi1* mutant has a foreign DNA insert in the third exon (Supplementary Figure S3A). Gene expression of *TWI1* is predicted to be disrupted, which was confirmed by RT-PCR (Supplementary Figure S3B). However, examination of the flagellar phenotype of *twi1* found that the mutant cells possess normal flagella and swim normally. These data suggest that TWI1 is unlikely involved in dynein arm assembly (Figure 6).

Discussion

In this study, we have characterized a *wdr92* mutant of *Chlamydomonas* to reveal its role and mechanism in dynein arm preassembly. The cytoplasmic localization of WDR92 and its effects on the stability of dynein heavy chains demonstrate that it functions in cytoplasmic preassembly of axonemal dyneins. WDR92 associates with multiple known factors involved in dynein preassembly. Most importantly, WDR92 interacts directly with a R2TP-like complex and associates with dynein heavy chains, suggesting that it participates in a process that recruits dynein heavy chains to the HSP90 co-chaperone R2TP-like complex to facilitate protein folding and assembly of dyneins. In addition, we showed that the three PIH1 domain-containing proteins PF13, MOT48, and TWI have different working mechanisms or functions.

The loss of axonemal dynein arms in the *wdr92* mutant is consistent with the results from studies in planaria and fly (Patel-King and King, 2016; Zur Lage et al., 2018). Interestingly, the short flagellar phenotype observed in this study was not reported before. IFT is required for proper cilia formation (Rosenbaum and Witman, 2002). The retrograde IFT requires cytoplasmic dynein 2/1b, loss of which results in very short flagella with bulged tips filled with IFT trains (Pazour et al., 1999; Porter et al., 1999). However, such a phenotype was not observed in the short flagella of *wdr92* (data not shown), indicating that WDR92 is unlikely involved in protein folding or assembly of the cytoplasmic dynein 2/1b. The short flagella phenotype is likely due to the instability of the axoneme caused by loss of axonemal dyneins (Lin et al., 2015). It has been shown that *Chlamydomonas* mutants lacking multiple axonemal dynein species often display shorter flagella (Huang et al., 1979; Piperno and Ramanis, 1991; Lin et al., 2015). Furthermore, the *pf13* and *mot48* double mutant, expected to lose both ODAs and IDAs, form extremely short flagella (Yamamoto et al., 2010). Thus, it appears that the presence of ODAs and IDAs is critical for axonemal microtubule stability or growth.

In human and zebrafish, there are four PIH1 domain-containing proteins that include PIH1D1, PIH1D2, PIH1D3, and DNAAF2/Ktu (Maurizy et al., 2018; Yamaguchi et al., 2018), whereas there are three PIH1 domain-containing proteins that include MOT48, PF13, and TWI1 in *Chlamydomonas* (Yamamoto et al., 2010). While PF13 and MOT48 mainly function in ODA and IDA assemblies, respectively, we found that TWI1 was not

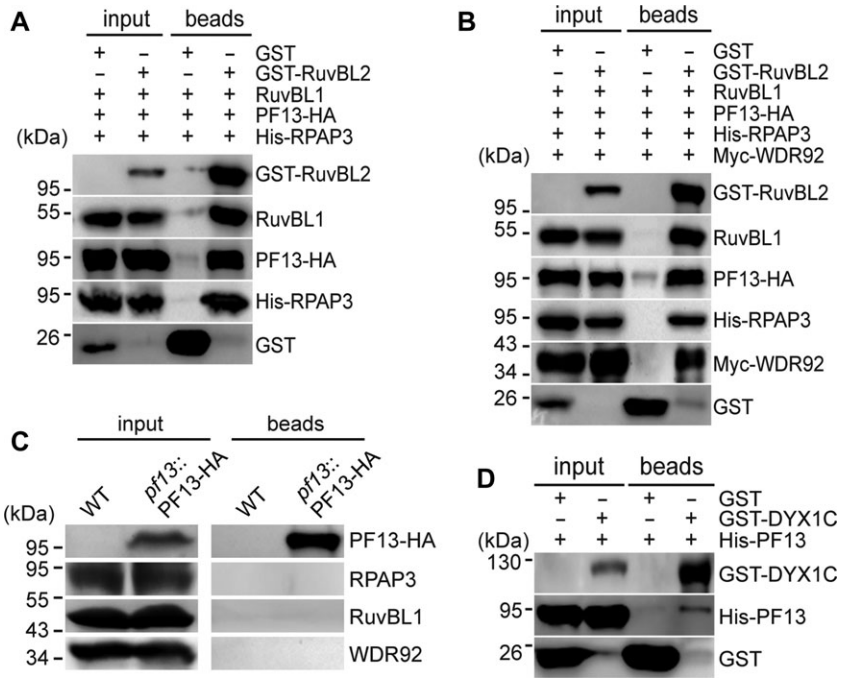

Figure 6 PF13, a PIH1 domain-containing protein, is involved in a R2TP-like complex formation *in vitro* but not *in vivo*. (**A** and **B**) GST pull-down assays show that PF13 is a component of a R2TP-like complex that interacts with WDR92. Bacterial expressed proteins were mixed together as indicated followed by GST pull-down and immunoblot analyses. PF13 forms a complex with RuvBL1/2 and RPAP3 (**A**), which interacts with WDR92 (**B**). (**C**) PF13 was not a component of a R2TP-like complex *in vivo*. Control cells or cells expressing PF13-HA were subjected to immunoprecipitation with the HA antibody followed by immunoblot analysis using the indicated antibodies. (**D**) PF13 interacts with DYX1C *in vitro*. Bacterial expressed proteins were subjected to GST pull-down assay as indicated.

involved in flagellar motility (Omran et al., 2008; Yamamoto et al., 2010; Mitchison et al., 2012). The divergent roles of the PIH1 domain-containing proteins in dynein arm assembly in *Chlamydomonas* are consistent with the findings in zebrafish (Yamaguchi et al., 2018). Phylogenetic analysis indicates that PF13 is a homolog of Ktu and TWI1 is closely related to vertebrate PIHD3 while MOT48 falls within a distinct clade (Yamaguchi et al., 2018). It appears that the homologs of the PIH1 domain-containing proteins in different organisms also have diverged functions. For example, in *pf13* mutant, the ODA assembly was mostly affected (Huang et al., 1979; Omran et al., 2008). However, in Medaka *ktu* mutant, both ODAs and IDAs are lost from the ciliary axoneme (Omran et al., 2008). Interestingly, only IDA assembly was slightly affected in a *ktu* mutant of zebrafish (Yamaguchi et al., 2018). Furthermore, *pihd3* null mutation results in partial loss of ODAs and IDAs in mouse sperm flagella whereas its null mutation in zebrafish induces complete loss of axonemal ODAs and some IDAs (Dong et al., 2014; Yamaguchi et al., 2018). In contrast, its homolog TWI1 is not involved in dynein assembly in *Chlamydomonas*.

The canonical R2TP complex is composed of RuvBL1/2, RPAP3, and PIH1D1. RPAP3 also has a paralogue, SPAG1, in the human proteome. PIH1D2 and Ktu both participate in R2TP-like complex formation (RuvBL1/2, SPAG1, and PIH1D2 or Ktu) (Maurizy et al., 2018). In addition, PIH1D3 and Ktu may also form an atypical R2TP complex (PIH1D3 or Ktu and DYX1C), which is also predicted from a recent report (Olcese et al., 2017). We have found that MOT48 was involved in R2TP-like complex formation *in vitro* and *in vivo*. Though PF13 was capable of forming a R2TP complex *in vitro*, this did not occur *in vivo*. However, we found that PF13 interacted with DYX1C *in vitro*. Based on the above data, we propose that MOT48 functions in dynein arm preassembly as a component of R2TP complex, while PF13 functions as a component of an atypical R2TP complex.

Our finding that WDR92 physically associates the R2TP-like complex to perform functions in dynein assembly is consistent with a recent report (Zur Lage et al., 2018). R2TP as a co-chaperone of HSP90 is involved in protein folding and assembly of multiple protein complexes (Kakihara and Houry, 2012). R2TP also associates with prefoldin-like (PFDL) module as well as with POLR2E and WDR92, which was proposed to form a complex termed PAQosome (particle for arrangement of quaternary structure) for its chaperone role in the assembly and maturation of protein complexes (Houry et al., 2018). In our studies, we did not find the association of WDR92 with the components of the PFDL module though they are present in the *Chlamydomonas* proteome (data not shown). In fly, WDR92 could pull down the components of PFDL module. However, none of these components function in the dynein assembly (Zur Lage et al., 2018).

WDR92 is required for the preassembly of both ODAs and IDAs, which can be explained by the functions of the associated

proteins. MOT48 and DYX1C/PF23 mainly functions in the IDA preassembly while ODA7 is involved in ODA preassembly (Yamamoto et al., 2010). What role does WDR92 exactly play in protein folding and preassembly of axonemal dyneins? WDR92 might be essential for assembling a complex involving R2TP-like complexes and other DNAAFs. Loss of WDR92 would disrupt the integrity of this complex and prevents recruiting nascent dynein polypeptides to chaperone HSP90 via the R2TP-like complex. Some of the WD repeats proteins interact with the group II chaperonin TCP-1 ring complex/chaperonin containing TCP-1 (Tric/CCT) for folding (Craig, 2003). Two components of the Tric/CCT including CCT2 and CCT8 were identified from immunoprecipitation of WDR92. This result might reflect folding of WDR92 via Tric/TTC. Another possibility is that WDR92 may bring dynein polypeptides that are associated with the WDR92 complex to Tric/CCT for folding. This suggestion, however, remains to be experimentally verified.

Materials and methods

Strains and culture

Chlamydomonas reinhardtii WT strain *21gr* (CC-1690, mt+), *pf13-3* (CC-4185, mt–), *ida10-1/mot48* (CC-4437, mt–), and *twi1* (LMJ.RY0402.076787, mt–) are available from the *Chlamydomonas* Resource Center (University of Minnesota, St. Paul, MN, USA). The *wdr92* mutant was generated from the WT strain by insertional mutagenesis in this study. Cells were grown in M liquid medium in Erlenmeyer flasks with aeration at 23°C in a 14/10 light/dark cycle (Sager and Granick, 1953; Zhu et al., 2017b). For transformation experiments, the cells were grown in liquid TAP medium under continuous light (Liang and Pan, 2013).

Insertional mutagenesis, gene cloning, and transformation

wdr92 was generated by transformation with electroporation of DNA fragments, which harbor expression cassette of paromomycin resistant gene *AphVIII* (Sizova et al., 2001). The flanking sequences of the DNA insert were identified by restriction enzyme site-directed PCR (RESDA-PCR) followed by sequencing (Gonzalez-Ballester et al., 2005). For gene complementation experiments, *WDR92, MOT48, TWI1* genes with an ~1.5 kb fragment upstream of the start codon were cloned respectively into the modified vector pHyg3 harboring a hygromycin B resistance gene with a YFP or 3× HA tag at the 3′ end (Berthold et al., 2002; Meng et al., 2014). For *pf13* complementation, a full-length cDNA for *PF13*, driven by PsaD promoter and tagged with a 3× HA tag at the 3′ end (Fischer and Rochaix, 2001), was also constructed into the modified vector pHyg3. The final constructs were linearized with ScaI and transformed into the respective mutants using electroporation (Liang and Pan, 2013). All the cDNAs used in this study were cloned from a *Chlamydomonas* cDNA library (TaKaRa). All the constructs were verified by sequencing.

Flagellar isolation and flagellar length measurement

A pH shock method was used for deflagellation followed by flagellar isolation (Craige et al., 2013; Zhu et al., 2017b). In brief, cells were deflagellated by pH shock followed by sucrose gradient centrifugation for further purification of the detached flagella. The isolated flagella were suspended in HMDEK buffer (50 mM HEPES, pH 7.2, 5 mM $MgCl_2$, 0.5 mM EDTA, 1 mM DTT, 25 mM KCl) containing protease inhibitor cocktail (mini-complete EDTA-free, Roche), flash frozen in liquid nitrogen and finally stored at –80°C until use. For flagellar length measurement or phenotypic examination, cells were fixed by 1% glutaraldehyde and imaged under the Zeiss Axio Observer Z1 differential interference contrast (DIC) microscope (Carl Zeiss) with a CCD camera (QuantEM512SC, Photometric).

RNA extraction and RT-PCR analysis

Total RNA extraction and RT-PCR were carried out following a previous publication (Liang et al., 2018). HiPure Plant RNA Mini Kit (Magen) was used for total RNA isolation and DNase I (NEB) for the elimination of genomic DNA following the manufacturer's instructions. cDNAs generated with the FastKing RT Kit (TIANGEN) were used as templates for PCR amplification. PCR primers were designed with Oligo 7 (www.oligo.net). *CBLP*, a gene encoding a G protein β subunit-like polypeptide, was used as a control. The primers used in RNA analysis are provided in Supplementary Table S2.

Yeast two-hybrid analysis

A previously published protocol was followed (Zhu et al., 2017a). The cDNAs used in this study were cloned into the yeast expression vector pGBKT7 containing a GAL4 binding domain (BD) and pGADT7 with the DNA activation domain (AD), respectively. Pair-wise combinations of the pGADT7 and pGBKT7 constructs were co-transformed into the yeast strain AH109. The transformants were grown at 30°C on selective medium SD lacking leucine, tryptophan, histidine, and adenine (SD, –Leu, –Trp, –His, –Ade) or lacking leucine and tryptophan (SD, –Leu, –Trp). Yeast cells co-transformed with the empty pGADT7 and pGBKT7 vectors were used as negative controls, while those co-transformed with the construct pair BD-53 plus AD-T as positive controls.

Antibodies

Details of the primary antibodies used for immunofluorescence and immunoblotting are provided in Supplementary Table S1. The polyclonal antibodies against WDR92, MOT48, RPAP3, and FBB18 were raised in rabbits, respectively (Abclone, China). The polypeptides used as antigens are the following: 51–337 aa for WDR92, 1–171 aa for MOT48, 1–240 aa for RPAP3 and a full-length polypeptide for FBB18. The polyclonal rabbit anti-DHCα and anti-DHCβ were kindly provided by Dr David Mitchell (SUNY Upstate Medical University), and anti-DHC5, anti-DHC8 and anti-DHC9 were kindly provided by Dr Toshiki Yagi (University of Tokyo).

The secondary antibodies of HRP-conjugated goat anti-mouse, goat anti-rabbit and goat anti-rat (1:5000, EASYBIO) were used for immunoblotting (IB), and the second antibodies of Texas red-conjugated goat anti-mouse IgG, Alexa Fluor 488

goat anti-rat (1:200, Life Technologies) were used for immunofluorescence (IF).

SDS-PAGE and immunoblotting

The SDS-PAGE and IB analysis have been described previously (Wu et al., 2018). Cells from liquid growing cultures were centrifuged at 13000 rpm for 2 min (Eppendorf 5417 R), flash frozen in liquid nitrogen and further stored at −80°C until use. The cells were lysed in Buffer A (50 mM Tris-HCl pH 7.5, 10 mM $MgCl_2$, 1 mM EDTA, 1 mM DTT) containing protease inhibitor cocktail (Roche) followed by centrifugation at 13000 rpm for 2 min at 4°C. The supernatant was boiled in 1× SDS sample buffer for 10 min, separated by SDS-PAGE, transferred to polyvinylidene difluoride (PVDF) membranes (Merck Millipore Ltd), and probed with the indicated antibodies.

IF and thin-section electron microscopy

IF analysis and thin-section electron microscopy have been described previously (Meng et al., 2014; Zhu et al., 2017b). For IF analysis, the cells were observed on a Zeiss LSM780 META Observer Z1 Confocal Laser Microscope. Images were processed by ZEN 2012 Light Edition (Zeiss) and Photoshop (Adobe). For electron microscopic analysis, the samples were imaged on an electron microscope (H-7650B; Hitachi Limited) equipped with a digital camera (ATM Company).

Immunoprecipitation and mass spectrometry analysis

Cells (1×10^9) were deflagellated by pH shock and allowed for flagellar regeneration for 15 min followed by cell collection for immunoprecipitation (IP). Cells were lysed with the IP buffer (20 mM HEPES, pH 7.2, 5 mM $MgCl_2$, 1 mM DTT, 1 mM EDTA, 20 mM β-glycerol phosphate, 10 mM NaF, 0.1 mM Na_3VO_4, 150 mM NaCl, 5% glycerol) containing protease inhibitor cocktail (complete-mini EDTA free, Roche). The supernatants obtained after centrifugation at 13000 rpm for 10 min at 4°C were cleared with 30 µl Protein A Sepharose (GE) for 30 min followed by incubation with 30 µl rat anti-HA Affinity Matrix (Roche) or anti-GFP Affinity Matrix (CMCTAG) for 4 h. The affinity matrixes were washed three times with the IP buffer containing 0.05% Tween-20 and one time with the IP buffer followed by boiling in 1× SDS sample. The samples were separated by SDS-PAGE followed by mass spectrometry analysis (Center of Biomedical Analysis, Tsinghua University) or immunoblotting.

Bacterial expression of recombinant proteins for pull-down assays

Full-length cDNAs for the *C. reinhardtii* genes were cloned into pGEX-6P-1 vectors, pET28a vectors, modified pETDuet-1 vectors or pRSFDuet-1 vectors followed by expression in *E. coli* Rosseta (DE3). The His-tag upstream of the MCS1 of the pETDuet-1 vector (kindly provided by Dr Xinquan Wang, Tsinghua University) was replaced with the GST-tag. The S-tag downstream of the MCS2 of the pRSFDuet-1 (from Dr Xinquan Wang) was replaced with the 3×HA-tag. *RuvBL1* without tag was cloned into the *Nde*I and *Xho*I sites and *RuvBL2* with a N-terminal GST-tag was cloned into the *Eco*RI and *Hin*dIII sites in pETDuet-1 vector. RPAP3 with a N-terminal 6×His-tag was cloned into the pRSFDuet-1 vector at *Bam*HI and *Hin*dIII sites while *MOT48, PF13, or TWI1* with a C-terminal 3×HA-tag was cloned into the same vector at *Nde*I and *Xho*I restriction sites, respectively. *RPAP3*, *PF13*, *MOT48*, *FBB18*, or *Oda7a* all with 6×His-tag at both ends was also cloned at *Nde*I and *Xho*I sites in pET28a vector, respectively. *WDR92* with a N-terminal GST-tag or with a N-terminal myc-tag was cloned into the pGEX-6P-1 vector at *Bam*HI and *Eco*RI sites or the pET28a vector at *Nde*I and *Xho*I sites, respectively. *RPAP3*, *DYX1C*, *Oda7a*, *Oda7b* with a N-terminal GST-tag was cloned into the pGEX-6P-1 vector.

Escherichia coli cultures were grown at 37°C with shaking at 200 rpm. The temperature was switched to 16°C when OD_{600} reached 2 and isopropyl-β-D-thiogalactopyranoside was added to a final concentration of 0.5 mM. The cells were collected 20 h later by centrifugation (1500× *g*, 10 min). The cell pellets were washed once with PBS buffer and stored at −80°C until use.

GST pull-down assay

The cells were lysed in PBS buffer containing 1 mM DTT and 1 mM PMSF by sonication (VCX500, Sonics & Materials) on ice. The lysates were cleared by centrifugation at 18000× *g* for 10 min. Glutathione beads (Smart Life Science) were mixed with the cleared cell lysates with rotation at 4°C for 4 h followed by washing three times with PBS buffer containing 0.1% Tween-20. Finally, the samples were analyzed by immunoblotting.

Supplementary material

Supplementary material is available at *Journal of Molecular Cell Biology* online.

Acknowledgements

We thank Drs Toshiki Yagi, David Mitchell, Kaiyao Huang, Robert Bloodgood, Xinquan Wang, and Dapeng Zhang for providing antibodies, plasmids, and/or strains. We also thank the Core Facility of the Center for Biomedical Analysis (Tsinghua University) for assistance on cell imaging and mass spectrometry analysis.

Funding

This work was supported by the National Key R&D Program of China (2017YFA0503500) and the National Natural Science Foundation of China (31330044 and 31671387) to J.P.

Conflict of interest: none declared.

Author contributions: G.L. and L.W. performed the experiments. J.P. provided reagents and facilities. G.L., L.W., and J.P. designed the experiments and analyzed the data. J.P. wrote the paper with contributions from G.L.

References

Ahmed, N.T., Gao, C., Lucker, B.F., et al. (2008). ODA16 aids axonemal outer row dynein assembly through an interaction with the intraflagellar transport machinery. J. Cell Biol. *183*, 313–322.

Balchin, D., Hayer-Hartl, M., and Hartl, F.U. (2016). In vivo aspects of protein folding and quality control. Science *353*, aac4354.

Berthold, P., Schmitt, R., and Mages, W. (2002). An engineered Streptomyces hygroscopicus aph 7″ gene mediates dominant resistance against hygromycin B in Chlamydomonas reinhardtii. Protist *153*, 401–412.

Boulon, S., Pradet-Balade, B., Verheggen, C., et al. (2010). HSP90 and its R2TP/Prefoldin-like cochaperone are involved in the cytoplasmic assembly of RNA polymerase II. Mol. Cell *39*, 912–924.

Cloutier, P., Al-Khoury, R., Lavallee-Adam, M., et al. (2009). High-resolution mapping of the protein interaction network for the human transcription machinery and affinity purification of RNA polymerase II-associated complexes. Methods *48*, 381–386.

Craig, E.A. (2003). Eukaryotic chaperonins: lubricating the folding of WD-repeat proteins. Curr. Biol. *13*, R904–R905.

Craige, B., Brown, J.M., and Witman, G.B. (2013). Isolation of Chlamydomonas flagella. Curr. Protoc. Cell Biol. *Chapter 3*, Unit 3.41.1–*9*.

Desai, P.B., Dean, A.B., and Mitchell, D.R. (2018). Cytoplasmic preassembly and trafficking of axonemal dyneins. In: King, S. (ed). Dyneins: The Biology of Dynein Motors. Cambridge, USA: Elsevier Inc., 141–161.

Dong, F., Shinohara, K., Botilde, Y., et al. (2014). Pih1d3 is required for cytoplasmic preassembly of axonemal dynein in mouse sperm. J. Cell Biol. *204*, 203–213.

Duquesnoy, P., Escudier, E., Vincensini, L., et al. (2009). Loss-of-function mutations in the human ortholog of Chlamydomonas reinhardtii ODA7 disrupt dynein arm assembly and cause primary ciliary dyskinesia. Am. J. Hum. Genet. *85*, 890–896.

Fischer, N., and Rochaix, J.D. (2001). The flanking regions of PsaD drive efficient gene expression in the nucleus of the green alga Chlamydomonas reinhardtii. Mol. Genet. Genomics *265*, 888–894.

Fok, A.K., Wang, H., Katayama, A., et al. (1994). 22S axonemal dynein is preassembled and functional prior to being transported to and attached on the axonemes. Cell Motil. Cytoskeleton *29*, 215–224.

Fowkes, M.E., and Mitchell, D.R. (1998). The role of preassembled cytoplasmic complexes in assembly of flagellar dynein subunits. Mol. Biol. Cell *9*, 2337–2347.

Gonzalez-Ballester, D., de Montaigu, A., Galvan, A., et al. (2005). Restriction enzyme site-directed amplification PCR: a tool to identify regions flanking a marker DNA. Anal. Biochem. *340*, 330–335.

Henri, J., Chagot, M.E., Bourguet, M., et al. (2018). Deep structural analysis of RPAP3 and PIH1D1, two components of the HSP90 co-chaperone R2TP complex. Structure *26*, 1196–1209.e8.

Hjeij, R., Onoufriadis, A., Watson, C.M., et al. (2014). CCDC151 mutations cause primary ciliary dyskinesia by disruption of the outer dynein arm docking complex formation. Am. J. Hum. Genet. *95*, 257–274.

Houry, W.A., Bertrand, E., and Coulombe, B. (2018). The PAQosome, an R2TP-based chaperone for quaternary structure formation. Trends Biochem. Sci. *43*, 4–9.

Huang, B., Piperno, G., and Luck, D.J. (1979). Paralyzed flagella mutants of Chlamydomonas reinhardtii. Defective for axonemal doublet microtubule arms. J. Biol. Chem. *254*, 3091–3099.

Ishikawa, T. (2017). Axoneme structure from motile cilia. Cold Spring Harb. Perspect. Biol. *9*, pii: a028076.

Itsuki, Y., Saeki, M., Nakahara, H., et al. (2008). Molecular cloning of novel Monad binding protein containing tetratricopeptide repeat domains. FEBS Lett. *582*, 2365–2370.

Jaffe, K.M., Grimes, D.T., Schottenfeld-Roames, J., et al. (2016). c21orf59/kurly controls both cilia motility and polarization. Cell Rep. *14*, 1841–1849.

Kakihara, Y., and Houry, W.A. (2012). The R2TP complex: discovery and functions. Biochim. Biophys. Acta *1823*, 101–107.

Kamiya, R., and Yagi, T. (2014). Functional diversity of axonemal dyneins as assessed by in vitro and in vivo motility assays of Chlamydomonas mutants. Zoolog. Sci. *31*, 633–644.

Kato, Y.S., Yagi, T., Harris, S.A., et al. (2014). Structure of the microtubule-binding domain of flagellar dynein. Structure *22*, 1628–1638.

King, S.M. (2016). Axonemal dynein arms. Cold Spring Harb. Perspect. Biol. *8*, pii: a028100.

Knowles, M.R., Ostrowski, L.E., Loges, N.T., et al. (2013). Mutations in SPAG1 cause primary ciliary dyskinesia associated with defective outer and inner dynein arms. Am. J. Hum. Genet. *93*, 711–720.

Li, Y., Zhao, L., Yuan, S., et al. (2017). Axonemal dynein assembly requires the R2TP complex component Pontin. Development *144*, 4684–4693.

Liang, Y., and Pan, J. (2013). Regulation of flagellar biogenesis by a calcium dependent protein kinase in Chlamydomonas reinhardtii. PLoS One *8*, e69902.

Liang, Y., Zhu, X., Wu, Q., et al. (2018). Ciliary length sensing regulates IFT entry via changes in FLA8/KIF3B phosphorylation to control ciliary assembly. Curr. Biol. *28*, 2429–2435.e3.

Lin, H., Zhang, Z., Guo, S., et al. (2015). A NIMA-related kinase suppresses the flagellar instability associated with the loss of multiple axonemal structures. PLoS Genet. *11*, e1005508.

Martino, F., Pal, M., Munoz-Hernandez, H., et al. (2018). RPAP3 provides a flexible scaffold for coupling HSP90 to the human R2TP co-chaperone complex. Nat. Commun. *9*, 1501.

Maurizy, C., Quinternet, M., Abel, Y., et al. (2018). The RPAP3-Cterminal domain identifies R2TP-like quaternary chaperones. Nat. Commun. *9*, 2093.

Meng, D., Cao, M., Oda, T., et al. (2014). The conserved ciliary protein Bug22 controls planar beating of Chlamydomonas flagella. J. Cell Sci. *127*, 281–287.

Mitchison, H.M., Schmidts, M., Loges, N.T., et al. (2012). Mutations in axonemal dynein assembly factor DNAAF3 cause primary ciliary dyskinesia. Nat. Genet. *44*, 381–389, S1–S2.

Olcese, C., Patel, M.P., Shoemark, A., et al. (2017). X-linked primary ciliary dyskinesia due to mutations in the cytoplasmic axonemal dynein assembly factor PIH1D3. Nat. Commun. *8*, 14279.

Omran, H., Kobayashi, D., Olbrich, H., et al. (2008). Ktu/PF13 is required for cytoplasmic pre-assembly of axonemal dyneins. Nature *456*, 611–616.

Paff, T., Loges, N.T., Aprea, I., et al. (2017). Mutations in PIH1D3 cause X-linked primary ciliary dyskinesia with outer and inner dynein arm defects. Am. J. Hum. Genet. *100*, 160–168.

Patel-King, R.S., and King, S.M. (2016). A prefoldin-associated WD-repeat protein (WDR92) is required for the correct architectural assembly of motile cilia. Mol. Biol. Cell *27*, 1204–1209.

Pazour, G.J., Dickert, B.L., and Witman, G.B. (1999). The DHC1b (DHC2) isoform of cytoplasmic dynein is required for flagellar assembly. J. Cell Biol. *144*, 473–481.

Piperno, G., and Ramanis, Z. (1991). The proximal portion of Chlamydomonas flagella contains a distinct set of inner dynein arms. J. Cell Biol. *112*, 701–709.

Porter, M.E., Bower, R., Knott, J.A., et al. (1999). Cytoplasmic dynein heavy chain 1b is required for flagellar assembly in Chlamydomonas. Mol. Biol. Cell *10*, 693–712.

Rivera-Calzada, A., Pal, M., Munoz-Hernandez, H., et al. (2017). The structure of the R2TP complex defines a platform for recruiting diverse client proteins to the HSP90 molecular chaperone system. Structure *25*, 1145–1152.e4.

Rosenbaum, J.L., and Witman, G.B. (2002). Intraflagellar transport. Nat. Rev. Mol. Cell Biol. *3*, 813–825.

Saeki, M., Irie, Y., Ni, L., et al. (2006). Monad, a WD40 repeat protein, promotes apoptosis induced by TNF-α. Biochem. Biophys. Res. Commun. *342*, 568–572.

Sager, R., and Granick, S. (1953). Nutritional studies with Chlamydomonas reinhardi. Ann. NY Acad. Sci. *56*, 831–838.

Sizova, I., Fuhrmann, M., and Hegemann, P. (2001). A Streptomyces rimosus aphVIII gene coding for a new type phosphotransferase provides stable antibiotic resistance to Chlamydomonas reinhardtii. Gene *277*, 221–229.

Te, J., Jia, L., Rogers, J., et al. (2007). Novel subunits of the mammalian Hsp90 signal transduction chaperone. J. Proteome Res. *6*, 1963–1973.

Wallmeier, J., Shiratori, H., Dougherty, G.W., et al. (2016). TTC25 deficiency results in defects of the outer dynein arm docking machinery and primary ciliary dyskinesia with left-right body asymmetry randomization. Am. J. Hum. Genet. *99*, 460–469.

Wu, Q., Gao, K., Zheng, S., et al. (2018). Calmodulin regulates a TRP channel (ADF1) and phospholipase C (PLC) to mediate elevation of cytosolic calcium during acidic stress that induces deflagellation in Chlamydomonas. FASEB J. *32*, 3689–3699.

Yagi, T., Uematsu, K., Liu, Z., et al. (2009). Identification of dyneins that localize exclusively to the proximal portion of Chlamydomonas flagella. J. Cell Sci. *122*, 1306–1314.

Yamaguchi, H., Oda, T., Kikkawa, M., et al. (2018). Systematic studies of all PIH proteins in zebrafish reveal their distinct roles in axonemal dynein assembly. Elife *7*, pii: e36979.

Yamamoto, R., Hirono, M., and Kamiya, R. (2010). Discrete PIH proteins function in the cytoplasmic preassembly of different subsets of axonemal dyneins. J. Cell Biol. *190*, 65–71.

Yamamoto, R., Obbineni, J.M., Alford, L.M., et al. (2017). Chlamydomonas DYX1C1/PF23 is essential for axonemal assembly and proper morphology of inner dynein arms. PLoS Genet. *13*, e1006996.

Zhang, Y., Chen, Y., Zheng, J., et al. (2019). Vertebrate Dynein-f depends on Wdr78 for axonemal localization and is essential for ciliary beat. J. Mol. Cell Biol. *11*, 383–394.

Zhao, R., Davey, M., Hsu, Y.C., et al. (2005). Navigating the chaperone network: an integrative map of physical and genetic interactions mediated by the hsp90 chaperone. Cell *120*, 715–727.

Zhao, L., Yuan, S., Cao, Y., et al. (2013). Reptin/Ruvbl2 is a Lrrc6/Seahorse interactor essential for cilia motility. Proc. Natl Acad. Sci. USA *110*, 12697–12702.

Zhu, X., Liang, Y., Gao, F., et al. (2017b). IFT54 regulates IFT20 stability but is not essential for tubulin transport during ciliogenesis. Cell. Mol. Life Sci. *74*, 3425–3437.

Zhu, B., Zhu, X., Wang, L., et al. (2017a). Functional exploration of the IFT-A complex in intraflagellar transport and ciliogenesis. PLoS Genet. *13*, e1006627.

Zur Lage, P., Stefanopoulou, P., Styczynska-Soczka, K., et al. (2018). Ciliary dynein motor preassembly is regulated by Wdr92 in association with HSP90 co-chaperone, R2TP. J. Cell Biol. *217*, 2583–2598.